# Extended imaging, deconvolution, and two-way wavefields: a comparison

*Esteban Díaz, Satyan Singh, and Paul Sava, Center for Wave Phenomena, Colorado School of Mines*

## SUMMARY

Multiple-scattered waves contain information that is commonly disregarded during imaging and tomography. Marchenko wavefields are superior to time-reverse wavefields by handling primaries together with internal and surface-related multiples. Using all types of waves for imaging can greatly improve the illumination and augment the sensitivity of the data to errors in the background velocity model. We compare extended images computed with reverse time and Marchenko wavefields, and investigate the potential of using multidimensional deconvolution for extended images in order to obtain higher image resolution. Our experiments show that the Marchenko wavefields are sensitive to errors in the background model in a way that is similar to the sensitivity of time-reverse wavefields. The main difference between these imaging strategies is the improved angle illumination with the Marchenko wavefields due to the correct use of multiples; this improvement can eliminate the bias of tomography operators towards lower velocities when the data are contaminated with multiples.

## INTRODUCTION

The quality of the seismic image depends on the choice of wave propagator, but more importantly on the quality of the background model. The better the velocity, the more focused the seismic image becomes. In order to retrieve the information about kinematics errors, one must extend the image. In the context of two-way operators, the extension is usually performed using extended images (Rickett and Sava, 2002; Sava and Fomel, 2006; Sava and Vasconcelos, 2011a), or the angle domain (Sava and Fomel, 2003; Yoon et al., 2004; Jin et al., 2014; Yoon et al., 2011; Vyas et al., 2011), or the surface offset domain (Giboli et al., 2012). Another important factor that determines the quality of a seismic image is the amount of data illuminating a target in the subsurface.

Most of the current imaging (and modeling) technologies utilize the primaries in the data but disregard the multiples which can better illuminate the targets with conventional acquisition geometries. In order to incorporate the multiples into the seismic images, a conventional approach is to use the primaries as an areal source for the surface-related multiples; this allows one to image the first order surface-related multiples in the same position as the primaries (Guitton, 2002; Grion et al., 2007; Verschuur and Berkhout, 2011; Whitmore et al., 2010; Wong et al., 2015). However, these techniques require prior separation of multiples and primaries. A recent alternative to incorporate the multiples into the imaging process is the Marchenko modeling framework in which the multiples are used together with the primaries in a global prediction procedure that characterizes focusing at an arbitrary location in the subsurface (Broggini et al., 2014; Behura et al., 2014; Wapenaar et al., 2014b; Singh et al., 2015). The focusing solutions are guaranteed to exist regardless of the background velocity model. With focusing functions, the up- and down-going Green's functions are retrieved through convolutions and correlations between the focusing solutions and the reflection response (the data) including internal multiples (Broggini et al., 2014; Behura et al., 2014; Wapenaar et al., 2014b) and surface-related multiples (Singh et al., 2015).

We show that the Marchenko wavefields contain sensitivity to the background model that is similar to conventional wavefields obtained by time reversal or downward continuation. We assess the sensitivity by using extended images, which is the first step towards a formulation of a tomographic operator with Marchenko wavefields. We also pose the extended imaging process as an inversion problem which can be thought of as an extended deconvolution imaging condition. We illustrate our method with synthetic examples comparing the sensitivity of both approaches to the background model.

## MODELING DIFFERENCES

In this section, we review similarities and differences between Marchenko and RTM propagators. While both propagators are two-way, Marchenko separates the total wavefield $u$ into up- and down-going components:

$$u(\mathbf{x},\mathbf{x}_s,t) = u_s(\mathbf{x},\mathbf{x}_s,t) + u_r(\mathbf{x},\mathbf{x}_s,t). \qquad (1)$$

This separation is necessary because the method relies on one-way reciprocity theorems (Wapenaar et al., 2014a). Singh et al. (2015) shows how to recover the total wavefield $u$, and its directional components $u_s$ and $u_r$ with a free-surface condition.

An iterative procedure finds the focusing solutions $f_1^+(\mathbf{x}_s,\mathbf{x},t)$ and $f_1^-(\mathbf{x}_s,\mathbf{x},t)$ such that when they are injected at the surface locations $\mathbf{x}_s$ produce a focus at an arbitrary point $\mathbf{x}$ in the subsurface. The focusing solutions always exist regardless of the background model. In order to obtain the focusing solutions, the method utilizes the reflectivity response $R(\mathbf{x}_s,\mathbf{x}_r,t)$ together with an estimate of the direct arrival $T_d(\mathbf{x},\mathbf{x}_r,t)$ which goes from the subsurface point $\mathbf{x}$ to the surface locations $\mathbf{x}_r$. The direct arrival information contains the kinematic information from the background model. The recovered wavefield satisfies the wave equation

$$\rho\nabla\cdot\left(\frac{1}{\rho}\nabla u\right) + \frac{\omega^2}{v^2}u = -j\omega\rho\delta(\mathbf{x}-\mathbf{x}_s) \qquad (2)$$

for a volumetric injection source $-j\omega\rho\delta(\mathbf{x}-\mathbf{x}_s)$, density $\rho$, and velocity $v$.

Once the focusing functions are obtained through the iterative scheme described in Singh et al. (2015), the individual components are then retrieved through the following equations:

$$u_r(\mathbf{x},\mathbf{x}_r,\omega) = -f_1^-(\mathbf{x}_r,\mathbf{x},\omega) + \sum_{\mathbf{x}_s} f_1^+(\mathbf{x}_s,\mathbf{x},\omega)\, R(\mathbf{x}_r,\mathbf{x}_s,\omega) - r f_1^-(\mathbf{x}_s,\mathbf{x},\omega)\, R(\mathbf{x}_r,\mathbf{x}_s,\omega), \quad (3)$$

$$u_s(\mathbf{x},\mathbf{x}_r,\omega) = +f_1^+(\mathbf{x}_r,\mathbf{x},\omega)^* - \sum_{\mathbf{x}_s} f_1^-(\mathbf{x}_s,\mathbf{x},\omega)^*\, R(\mathbf{x}_r,\mathbf{x}_s,\omega) - r f_1^+(\mathbf{x}_s,\mathbf{x},\omega)\, R(\mathbf{x}_r,\mathbf{x}_s,\omega). \quad (4)$$

Note that the inputs for retrieving either wavefield are the same: the focusing solutions $f_1^+$ and $f_1^-$, the reflectivity at the surface $R$ (the data), and the reflection coefficient at the free surface $r=-1$. The focusing solutions $f_1^-$ and $f_1^+$ can be thought of as the propagators that redatum the reflectivity from the source position $\mathbf{x}_s$ to the image point $\mathbf{x}$.

In contrast, the RTM propagators solve two independent modeling problems:

$$L(v)u_s = f_s, \quad (5)$$

which is solved forward in time for the source function $f_s$, and

$$L^\top(v)u_r = f_r, \quad (6)$$

which is solved backward in time for the receiver data $f_r = \sum_{\mathbf{x}_r} R(\mathbf{x}_s,\mathbf{x}_r,t)\delta(\mathbf{x}-\mathbf{x}_r)$. For the RTM propagators, the sum of the source and receiver wavefields does not satisfy equation 2 and does not correctly handle the multiples present in the data.

## SENSITIVITY TO THE BACKGROUND MODEL

In the Marchenko context, the wavefield $u_r$ represents the up-going component of the Green's function, whereas $u_s$ represents the downgoing component. Following the imaging principle (Claerbout, 1971) the image $R(\mathbf{x})$ is constructed when wavefields $u_s$ and $u_r$ coincide in space and time:

$$R(\mathbf{x}) = \sum_{\mathbf{x}_s,t} u_s(\mathbf{x}_s,\mathbf{x},t)u_r(\mathbf{x}_s,\mathbf{x},t). \quad (7)$$

Although helpful for understanding the subsurface, $R(\mathbf{x})$ does not contain much information about the quality of the background velocity model. Instead, one can use the extended-imaging condition (Rickett and Sava, 2002; Sava and Fomel, 2003; Sava and Vasconcelos, 2011b) to analyze the interaction between source and receiver wavefields at the vicinity of the image location $\mathbf{x}$ and $t=0$:

$$R(\mathbf{x},\boldsymbol{\lambda},\tau) = \sum_{e,t} u_s(e,\mathbf{x}-\boldsymbol{\lambda},t-\tau)u_r(e,\mathbf{x}+\boldsymbol{\lambda},t+\tau), \quad (8)$$

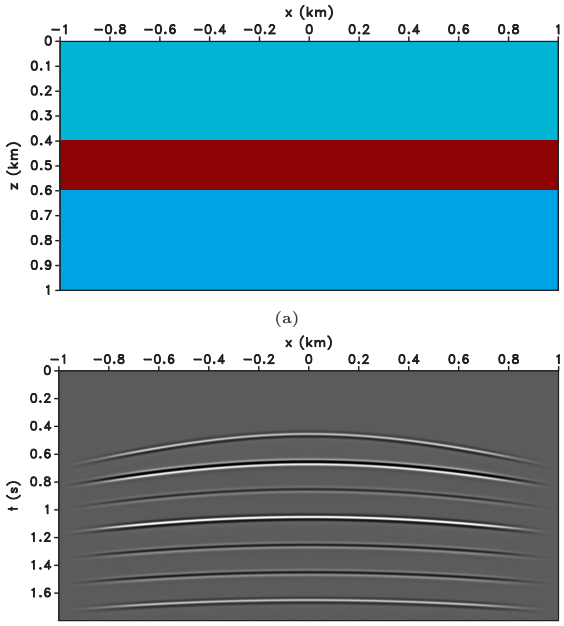


(a)

(b)

Figure 1: Free surface experiment with a constant velocity background: (a) variable density model and (b) the recorded data for a shot at $\mathbf{x}_s = (0,0)$km. Note how the data contain primaries, internal and surface-related multiples.

where $\boldsymbol{\lambda}$ and $\tau$ are space- and time-lags, respectively. The extended-imaging operator is linear and represents the down-going field, $u_s$, interacting with the up-going field, $u_r$; which in a matrix-vector form it reads

$$R = \mathbf{U_s}^\top u_r, \quad (9)$$

where, the matrix $\mathbf{U_s}^\top$ is the extended-imaging operator applied to the receiver field $u_r$. Alternatively, one can think about the (extended) imaging process as an inversion problem such that $R(\mathbf{x},\boldsymbol{\lambda},\tau)$ satisfies the relation

$$\mathbf{U_s} R \approx u_r, \quad (10)$$

where the operator $\mathbf{U_s}$ implements:

$$\tilde{u_r}(\mathbf{x}_s,\mathbf{x},t) = \sum_{\tau,\boldsymbol{\lambda}} R(\mathbf{x}-\boldsymbol{\lambda},\boldsymbol{\lambda},\tau)u_s(\mathbf{x}_s,\mathbf{x}-2\boldsymbol{\lambda},t+2\tau). \quad (11)$$

The wavefield $\tilde{u_r}$ denotes the action of $\mathbf{U_s}$ applied to $R$. The relation in equation 10 implies that the extended reflectivity $R(\mathbf{x},\boldsymbol{\lambda},\tau)$ is the ratio between the down- and up-going fields at the surrounding locations of image point $\mathbf{x}$ and around time $t=0$ (Wapenaar et al., 2000; Amundsen, 2001). In order to stabilize the inversion, we add a damping constrain by keeping the extended reflectivity as small as possible:

$$\epsilon R \approx 0. \quad (12)$$

The composite system can be written as

$$\left(\mathbf{U_s}^\top \mathbf{U_s} + \epsilon^2 \mathbf{I}\right) R = \mathbf{U_s}^\top u_r, \quad (13)$$

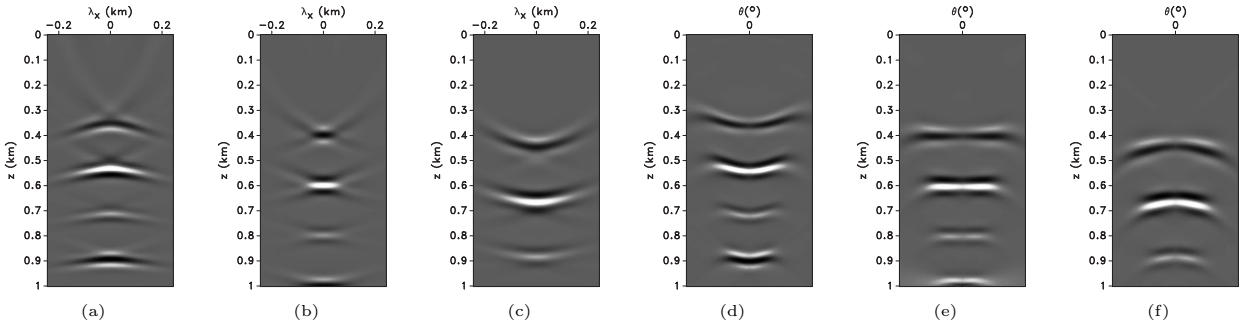


Figure 2: Space-lag gathers obtained from RTM wavefields for (a) low, (b) correct, and (c) fast velocity. Corresponding angle gathers for (d) low, (e) correct, and (f) fast velocity.

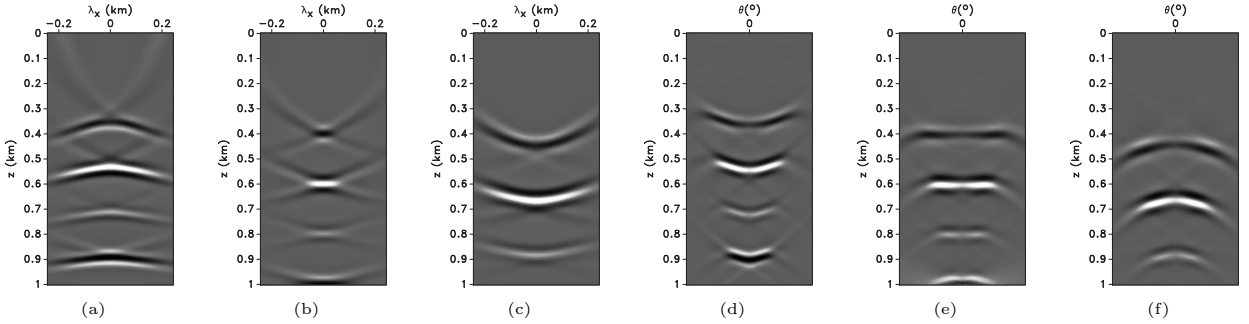


Figure 3: Deconvolved space-lag gathers obtained from RTM wavefields for (a) low, (b) correct, and (c) fast velocity. Corresponding deconvolved angle gathers for (d) low, (e) correct, and (f) fast velocity.

and can be solved by the conjugate gradient method. Note that the matrix $\mathbf{U_s^\top U_s}$ does not need to be formed; instead one needs to compute the action of the matrix to the input reflectivity $R(\mathbf{x}, \boldsymbol{\lambda}, \tau)$. The deconvolution process is similar to the method proposed by Valenciano et al. (2009) and is also referred to as multi-dimensional deconvolution (MDD) by van der Neut et al. (2011). The deconvolution approach produces better focusing and better approximates the reflectivity.

## EXAMPLES

We compare the behavior of RTM and Marchenko images for errors in the background velocity using a synthetic model with constant background velocity and variable density profile, Figure 1a. The pressure data containing primaries and multiples is shown in Figure 1b. Our main objective is to investigate the sensitivity of the Marchenko images to errors in the background model, which is the first step towards the formulation of a tomography problem.

We construct extended images with $\tau = 0$, i.e. space-lag gathers, for slow, correct, and fast background velocities. Figures 2a-2c show the gathers computed using the conventional RTM propagator, where one can observe the strong response of the multiples present in the data below the imaged reflector. Figures 2d-2f show the corresponding common angle gathers for slow, correct, and fast models, respectively. The transformation from space-lag $\boldsymbol{\lambda}$ to angle $\theta$ is described by Sava and Fomel (2006). For this particular model, the reflection coefficient should remain constant as a function of the scattering angle. We recompute the same set of images with the deconvolution framework in equation 13: Figures 3a-3c show the deconvolved space-lag gathers with RTM wavefields, and Figures 3d-3f show the corresponding angle gathers with the RTM wavefields. In these figures, the amplitude variation across angles is more even. The deconvolved space-lag gathers contain more energy at larger lags; this can be beneficial for improved tomographic updates because during tomography, the objective function measures the energy away from $\boldsymbol{\lambda} = 0$ (Shen and Symes, 2008). Hence, with the deconvolved gathers one can better highlight aspects of the gathers useful for tomography.

We repeat the same experiment using the Marchenko wavefields. Figures 4a-4c show the space-lag gathers for low, correct, and fast background velocity, respectively. The main difference between these gathers and those in Figures 2a-2c is the correct handling of the surface-related and internal multiples. Despite the characteristics of the method, where the focusing solutions $f_1^+$ and $f_1^-$ always exist, the gathers present moveout, indicating errors in the background model. Also, the focusing for the correct velocity model, Figure 4b, is improved

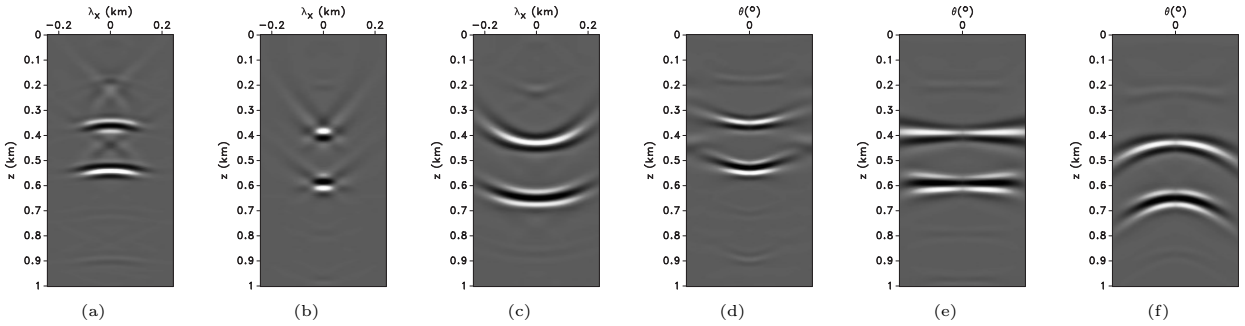


Figure 4: Space-lag gathers obtained from Marchenko wavefields for (a) low, (b) correct, and (c) fast velocity. Corresponding angle gathers for (d) low, (e) correct, and (f) fast velocity.

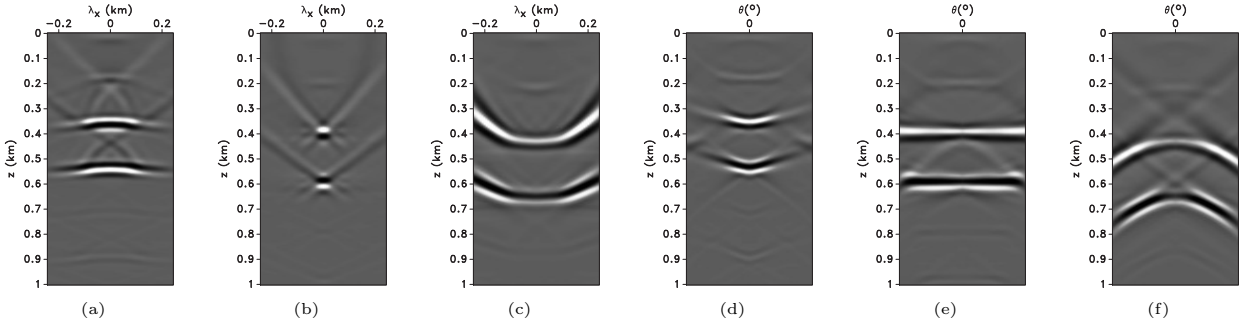


Figure 5: Deconvolved space-lag gathers obtained from Marchenko wavefields for (a) low, (b) correct, and (c) fast velocity. Corresponding deconvolved angle gathers for (d) low, (e) correct, and (f) fast velocity. The angle amplitude is more even for the deconvolved gathers, and the focus for correct velocity is much better than in Figure 4b.

when compared to Figure 2b. The better focusing is due to the improved illumination achieved by incorporating surface-related and internal multiples in the final image. The angle gathers from Figures 4d-4f show a stronger response at the near angles. After deconvolving the Marchenko gathers (Figures 5a-5c) , the focus greatly improves, which can be better appreciated with the correct velocity case, Figure 5b. We also see the same pattern as with Figures 3a-3c where the energy spreads more evenly over space-lags. The angle gathers (Figures 5d-5f) show a better amplitude response.

## CONCLUSIONS

We compare image gathers obtained with Marchenko and time-reverse propagators. The Marchenko gathers correctly image primaries, internal multiples, and surface-related multiples. In contrast, RTM gathers treat the multiples as primaries; hence, the events are imaged in the wrong location and can bias tomographic inversion towards lower velocities. The Marchenko and RTM gathers show similar sensitivity to errors in the background model. However, the Marchenko gathers possess increased illumination as shown by the angle gathers in our experiments.

We also show the value of posing the extended imaging problem using deconvolution instead of correlation. The focus in the gather is improved, and the energy distribution is more homogeneous across angles. The use of Marchenko wavefields together with extended deconvolution can benefit tomography. The dependence of the Marchenko wavefield with respect to the background velocity is not as explicit as with the RTM wavefields; in Marchenko, the kinematics are embedded in the direct arrival information used as input for the framework.

## ACKNOWLEDGMENTS

We thank the sponsors of the Center for Wave Phenomena, whose support made this research possible. The reproducible numeric examples in this paper use the Madagascar open-source software package (Fomel et al., 2013) freely available from http://www.ahay.org.

## REFERENCES


Amundsen, L., 2001, Elimination of freesurface related multiples without need of the source wavelet: GEOPHYSICS, **66**, 327–341.

Behura, J., K. Wapenaar, and R. Snieder, 2014, Autofocus imaging: Image reconstruction based on inverse scattering theory: Geophysics, **79**, A19–A26.

Broggini, F., R. Snieder, and K. Wapenaar, 2014, Data-driven wavefield focusing and imaging with multidimensional deconvolution: Numerical examples for reflection data with internal multiples: Geophysics, **79**, WA107–WA115.

Claerbout, J. F., 1971, Toward a unified theory of reflector mapping: Geophysics, **36**, 467–481.

Fomel, S., P. Sava, I. Vlad, Y. Liu, and V. Bashkardin, 2013, Madagascar: open-source software project for multidimensional data analysis and reproducible computational experiments: Journal of Open Research Software, **1**, e8.

Giboli, M., R. Baina, L. Nicoletis, and B. Duquet, 2012, Reverse time migration surface offset gathers part 1: a new method to produce classical common image gathers: 1–5.

Grion, S., R. Exley, M. Manin, X. Miao, A. Pica, Y. Wang, P. Granger, and S. Ronen, 2007, Mirror imaging of obs data: first break, **25**.

Guitton, A., 2002, Shotprofile migration of multiple reflections: SEG Technical Program Expanded Abstracts 2002, 1296–1299.

Jin, H., G. A. McMechan, and H. Guan, 2014, Comparison of methods for extracting adcigs from rtm: Geophysics, **79**, S89–S103.

Rickett, J. E., and P. C. Sava, 2002, Offset and angle-domain common image-point gathers for shot-profile migration: Geophysics, **67**, 883–889.

Sava, P., and S. Fomel, 2006, Time-shift imaging condition in seismic migration: Geophysics, **71**, S209–S217.

Sava, P., and I. Vasconcelos, 2011a, Extended imaging conditions for wave-equation migration: Geophysical Prospecting, **59**, 35–55.

———, 2011b, Extended imaging conditions for wave-equation migration: Geophysical Prospecting, **59**, 35–55.

Sava, P. C., and S. Fomel, 2003, Angle-domain common-image gathers by wavefield continuation methods: Geophysics, **68**, 1065–1074.

Shen, P., and W. W. Symes, 2008, Automatic velocity analysis via shot profile migration: Geophysics, **73**, VE49–VE59.

Singh, S., R. Snieder, J. Behura, J. van der Neut, K. Wapenaar, and E. Slob, 2015, Marchenko imaging: Imaging with primaries, internal multiples, and free-surface multiples: Geophysics, **80**, S165–S174.

Valenciano, A. A., B. L. Biondi, and R. G. Clapp, 2009, Imaging by target-oriented wave-equation inversion: Geophysics, **74**, WCA109–WCA120.

van der Neut, J., J. Thorbecke, K. Mehta, E. Slob, and K. Wapenaar, 2011, Controlled-source interferometric redatuming by crosscorrelation and multidimensional deconvolution in elastic media: Geophysics, **76**, SA63–SA76.

Verschuur, D. J. E., and A. J. G. Berkhout, 2011, Seismic migration of blended shot records with surface-related multiple scattering: Geophysics, **76**, A7–A13.

Vyas, M., D. Nichols, and E. Mobley, 2011, Efficient rtm angle gathers using source directions: 3104–3108.

Wapenaar, K., J. Fokkema, M. Dillen, and P. Scherpenhuijsen, 2000, Oneway acoustic reciprocity and its applications in multiple elimination and timelapse seismics: SEG Technical Program Expanded Abstracts 2000, 2377–2380.

Wapenaar, K., J. Thorbecke, J. van der Neut, F. Broggini, E. Slob, and R. Snieder, 2014a, Green's function retrieval from reflection data, in absence of a receiver at the virtual source position: The Journal of the Acoustical Society of America, **135**, 2847–2861.

———, 2014b, Marchenko imaging: Geophysics, **79**, WA39–WA57.

Whitmore, N. D., A. A. Valenciano, W. Sollner, and S. Lu, 2010, Imaging of primaries and multiples using a dualsensor towed streamer: SEG Technical Program Expanded Abstracts 2010, 3187–3192.

Wong, M., B. L. Biondi, and S. Ronen, 2015, Imaging with primaries and free-surface multiples by joint least-squares reverse time migration: Geophysics, **80**, S223–S235.

Yoon, K., M. Guo, J. Cai, and B. Wang, 2011, 3d rtm angle gathers from source wave propagation direction and dip of reflector: SEG Technical Program Expanded Abstracts 2011, 3136–3140.

Yoon, K., K. J. Marfurt, and W. Starr, 2004, Challenges in reversetime migration: SEG Technical Program Expanded Abstracts, 1057–1060.